Governing Rule for Dynamic Formation of Grain Boundaries in Grown Graphene

Wei Guo,[†,‡,⊥] Bin Wu,[†,⊥] Yongtao Li,[†] Lifeng Wang,[†] Jisi Chen,[†] Bingyan Chen,[§] Zhiyong Zhang,[§] Lianmao Peng,[§] Shuai Wang,[*,‡] and Yunqi Liu[*,†]

[†]Beijing National Laboratory for Molecular Sciences, Key Laboratory of Organic Solids, Institute of Chemistry, Chinese Academy of Science, Beijing 100190, People's Republic of China, [‡]School of Chemistry and Chemical Engineering, Huazhong University of Science & Technology, Wuhan 430074, People's Republic of China, and [§]Key Laboratory for the Physics and Chemistry of Nanodevices, Department of Electronics, Peking University, Beijing 100871, People's Republic of China. [⊥]W. Guo and B. Wu contributed equally.

ABSTRACT Grains and grain boundaries (GBs) in graphene are vital for the control of its properties; however, engineering or controlling them by growth remains a great challenge. Here we discover that the dynamic formation of GBs within chemical vapor deposited polygonal graphene flakes is described by a geometric rule. A GB is formed to be symmetrically tilted and a continuous straight line, and the key parameters including end point, direction of GB line, and misorientation angles between adjacent graphene grains can be determined solely by the geometries of the polygonal graphene flakes. We also show the growth control over the length of straight graphene GB lines and demonstrate the capability of parallel fabrication of field-effect transistor devices across predicted GBs in a straightforward manner. This work constitutes a significant step forward in engineering grains and GBs in graphene.

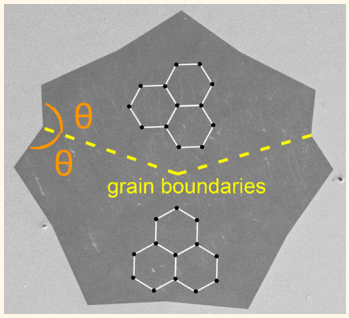

KEYWORDS: grain boundaries · graphene · dynamic formation · chemical vapor deposition · anisotropic etching

Graphene is a two-dimensional material showing many excellent properties as a result of its unique structure.[1] Grain boundaries (GBs) within graphene act as intrinsic structural elements that can markedly alter the electronic[2−6] and mechanical properties.[7−10] Understanding how GBs in graphene are dynamically formed during the growth is critical to the development of graphene materials with controlled GB structure/profile and their related applications in functional electronic devices. Early studies have focused mainly on developing GB visualization methods[11,12] or probing the structure and properties of GBs in graphene[13−17] or MoS_2[18,19] materials grown by the chemical vapor deposition (CVD) method; however, much less is known about the basic formation process of GBs in typical CVD graphene growth. To date, it has been intuitively speculated that formed GB patterns may be related to specific growth methods, but GBs observed within graphene appear exceptionally complex and randomly distributed, posing a great challenge for further studying this key issue. As a result, probing GB properties unavoidably involves the use of time-consuming and intercoordinated techniques for GB identification and subsequent device fabrication.[6] On the other hand, there is no pathway for engineering GBs of graphene or achieving multiple GB-based devices in a straightforward manner at present.

Here we quantitatively elucidate the dynamic GB formation in the system of typical chemical vapor deposited polygonal graphene flakes (GFs) by experimental and theoretical modeling studies, demonstrating that GB formation follows a geometric rule. A symmetric tilt GB is formed as a continuous straight line in polygonal GFs, and both the GB profile and the corresponding misorientation angles between adjacent graphene grains have a direct correlation with the geometries of polygonal GFs. This provides a highly effective method for identification of these key parameters without the need for relying on any special techniques. We also show the growth control over the length of straight graphene GB lines and demonstrate the capability of parallel

* Address correspondence to liuyq@iccas.ac.cn, chmsamuel@hust.edu.cn.

Received for review January 11, 2015 and accepted May 19, 2015.

Published online May 19, 2015
10.1021/acsnano.5b01827

fabrication of field-effect transistor (FET) devices across predicted GBs in a straightforward manner.

RESULTS AND DISCUSSION

Isolated GFs including monolayer hexagonal (Figure 1a and Figure S1) and various-shaped polygonal GFs (Figure 1b,c and Figure S2) were grown on both solid and liquid Cu at temperatures from 1070 to 1100 °C by a CVD method at ambient pressure (see Methods).[20−22] Under a wide range of experimental conditions (for example, using different Ar/H_2 flow rate ratios and temperatures), the growth generally resulted in a dominant distribution of monolayer hexagonal GFs together with a small portion of monolayer polygonal GFs before the formation of a continuous graphene film. The existence of these symmetric or asymmetric polygonal GFs is insensitive to various growth conditions, indicating that a certain governing rule controls the growth process and apparent GF shapes. In order to study the general GB formation mechanism in this typical graphene CVD growth process, we first developed a method involving graphene anisotropic etching to probe the existence, distribution, and profile of GBs in these samples. In a fixed H_2/Ar mixed atmosphere, the etching of as-grown GFs on a Cu surface is exclusively anisotropic, resulting in etched hexagons with zigzag (ZZ) edges.[23−25] Therefore, the existence of GBs within graphene can be determined simply by observing the deviation of etched holes from the geometric parameters of a hexagon.

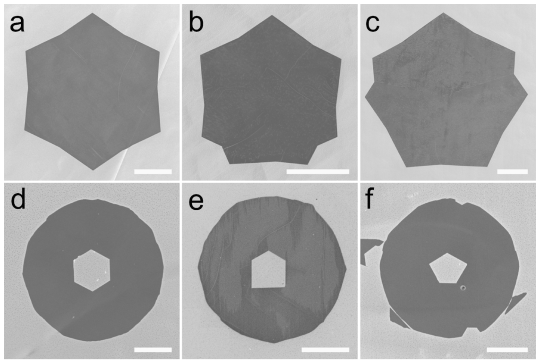

Figure 1. Morphology of CVD-grown and etched GFs. (a−c) Scanning electron microscopy (SEM) images of hexagonal and various polygonal-shaped GFs on Cu. (d−f) Morphologies of etched patterns with hexagonal and various polygonal shapes on GFs. The scale bars are 100 μm in a−c, 50 μm in d−f.

Figure 1d−f and Figure S3 show the typical cases in which only one or two etched patterns were observed on a single GF. Typically, in addition to hexagonal etched hole (Figure 1d), etched patterns exhibit various polygonal shapes, indicating the presence of GBs in polygonal GFs. We further analyzed the cases where multietched holes are formed on a single GF. In the case of etching on hexagonal GFs, all the etched holes are hexagons that are aligned in the same direction and with the edges of GFs (Figure 2a), which is consistent with the fact that hexagonal GFs are single crystalline with ZZ edges.[5] In contrast, the etching on polygonal GFs (Figure 2b−e and Figure S4a−c) shows different features including that (1) etched hexagons can be divided into different regions according to their relative alignment and (2) certain edges of etched polygons are aligned with those of polygonal GFs (Figure 2b) and those of adjacent etched hexagons. In the absence of adjacent etched hexagon (Figure 2c), the angles between labeled edges 1 and 2 or 2 and 3 are equal to 120°.

These observations essentially confirm the existence of grains and GBs in polygonal GFs. Therefore, in principle, we can conclude that if etched holes cross a part of a continuous GB in a GF, the locations on GB must be corresponding to a certain vertex of an etched polygon where the associated angles are not equal to 120°. On the basis of this principle, several dashed lines are drawn on GFs in Figure 2b−e, indicating possible grains and a GB configuration based on two or more such vertexes. Note that if the vertexes of a polygonal GF are related to non-120° angles, they are the natural

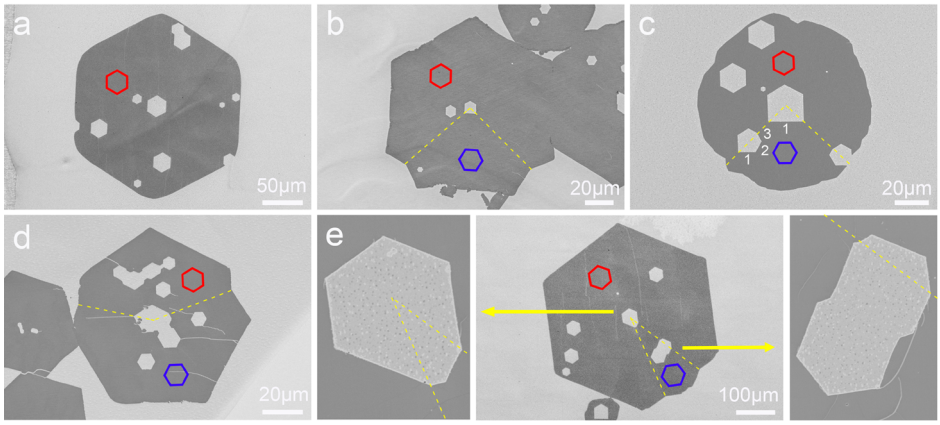

Figure 2. Etched patterns and GBs within GFs. (a) SEM images of multietched holes on a single-crystal hexagonal GF and on polygonal GFs (b−e), respectively. The red and blue hexagons are shown in each image to indicate the orientation of the etched hole. The close-up SEM images of etched patterns in the middle of (e) are shown on the left and right, respectively.

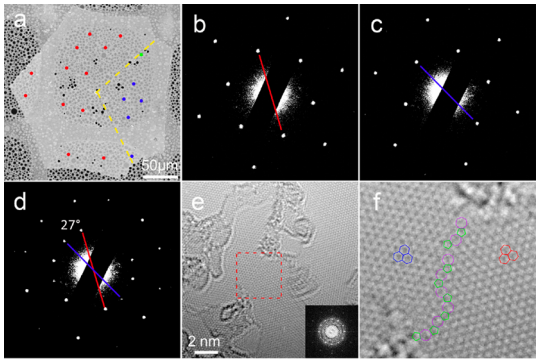

Figure 3. TEM characterization of hexagonal and polygonal GFs. (a) SEM image of a polygonal GF transferred on a TEM grid. The yellow dash lines indicate possible paths of existing GBs. (b–d) Typical SAED patterns obtained from the red dots (b), blue dots (c), and green dot (d) in (a), respectively. (e) HR-TEM image of grains and GBs within the GF. Inset at the right bottom is the Fourier transform image for the red dashed rectangle region. (f) Zoom-in image of the red dashed rectangle region in (e). Blue and red hexagons illustrate the crystal orientation of the two adjacent grains, and the most likely GB structure is outlined by purple heptagon and green pentagon pairs.

points on a GB. This finding demonstrates the capability of the etching for visualizing discontinuous locations of graphene grains and GBs, which is complementary to the family of graphene visualization methods.

We further conducted high-resolution transmission electron microscopy (HR-TEM) and selected area electron diffraction (SAED) techniques to characterize the crystal structure and GBs of polygonal GFs. Hexagonal GFs were confirmed to be single crystalline by the observation of only one set of 6-fold symmetric diffraction patterns (Figure S5). In contrast, different sets of rotated SAED patterns were observed across certain lines in various-shaped polygonal GFs, demonstrating that the whole flakes consist of separated grains (Figure 3a–d and Figures S6–S8). The aberration-corrected HR-TEM image in Figure 3e further confirms the existence of a continuous tilt GB at the atomic scale. Detailed atomic structures of a grain and a GB are shown in Figure 3f, where the marked blue and red hexagons depict the crystal orientation of the two grains, about 27° relatively tilted. The GBs at an atomic length scale are jagged. The structure of the GB is drawn in the image, showing alternating pentagons (green) and heptagons (purple), similar to the theoretical predictions[26,27] and experimental observations.[13–15]

To probe the entire path of the GB curve at a micrometer scale, we found that grains and GBs of polygonal GFs grown on Cu with mild air oxidation can be easily identified by SEM imaging (Figure S9), and this technique is similar to cases of direct visualization with optical images.[11,12,28] Note that Raman spectra for transferred GFs before and after air oxidation (Figure S10) show similar results without the presence of detectable D peaks. Our method was then used to directly visualize the shapes and locations of GBs within GFs (Figure S11), and in all cases, GBs were observed to be continuous and straight lines.

Using the above developed techniques, the GB parameters such as existence, profile, and structure in CVD-grown polygonal GFs can be known. However, this trial and error approach, which was indeed adopted in previous work, is individual phenomenon-based, and it is essential to find out the basic principle of GB formation operating in all phenomena. We have carefully analyzed the GB formation process in this growth system. There are three possible mechanisms of GB formation during the growth of graphene. First, a multiple nucleation event occurs almost at the same place during a short period of time. GBs will then grow with graphene grain growth. Second, a single nucleus is formed, and during its growth, new nucleation may occur on the edges of the growing GF by statistical fluctuation or other means. Further simultaneous growth of both "large mother" and "small son" nuclei results in the formation of GBs if two nuclei are misoriented. Finally, two grown GFs meet and then experience a coalescence process that is responsible for the formation of GBs and the continuous film. We can thus establish a geometric model to describe the GB formation independently by the use of the anisotropic growth principle and treating other parameters such as the number of nuclei, the relative orientation of nuclei, the nucleation time, and location as variables, allowing the quantitative description of the whole GB formation process.

Figure 4a shows two models describing the GB formation process of two kinds of typical polygonal GFs. In the case of the left model, the central hexagon represents the growing GF with a second nucleation event occurring on one of its edges. The new nucleus is defined to have a different orientation from the growing one. By applying the anisotropic growth rule (graphene growth rate along the armchair (AC) edge on Cu is faster than that of the ZZ edge on Cu[29,30]) to both the large growing GF and the new small nucleus, the growth rate along the AC direction (V_{AC}) for the former is equal to that for the latter (the left model of Figure 4a). Then, during the growth, the shape and relative orientation of both large and small hexagonal GFs remain the same, and their outer edges will have intersection points that define the periphery points of the entire "composite" GF. The morphology of polygonal GFs at any growth stage can thus be constructed by repeating this process. This construction process naturally identifies the landscape of GBs in polygonal GFs as shown in black lines on the left in Figure 4a. The right model of Figure 4a shows a case where multiple nuclei on a location grow based on a similar construction process. Many other models are shown in Figure S12. It is very clear that the observed morphologies of polygonal GFs can be perfectly reproduced from these models. Two typical growth processes for

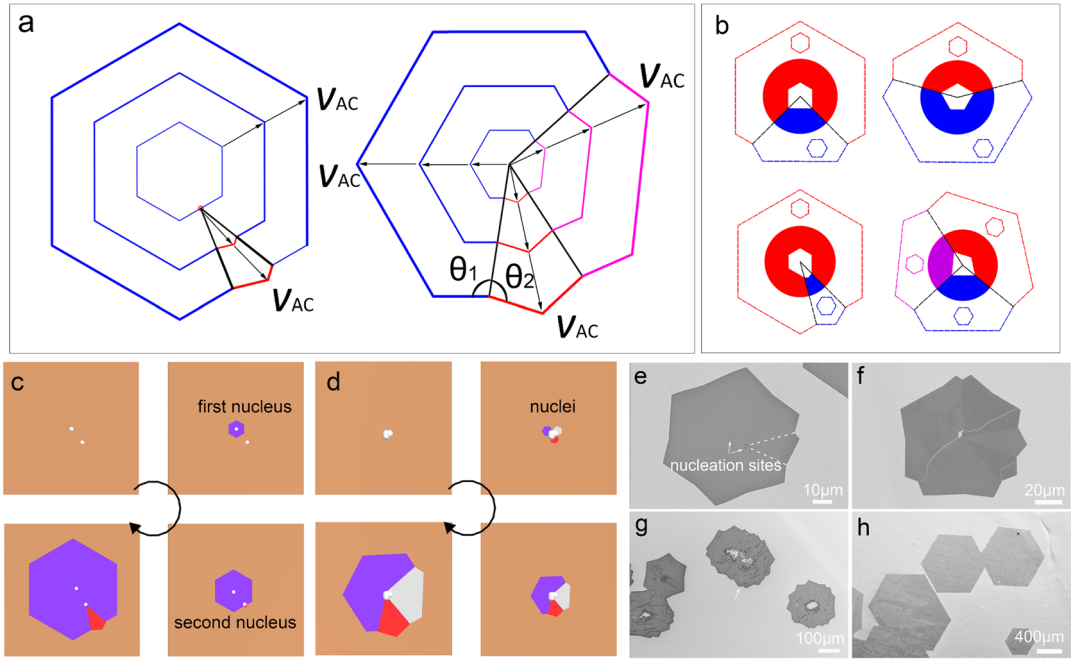

Figure 4. Modeling the formation mechanism of GBs in polygonal GFs and comparing models with experimental results. (a) The left model shows the construction process of a polygonal GF using the anisotropic growth rule. In this case, a second nucleus (red) is formed on one edge of a central growing hexagon (blue). Equal growth rate along the AC direction (V_{AC}) for both nuclei is indicated in (a). The right model shows the formation of a polygonal GF containing three grains nucleated at the same location. In both models, black lines define the paths of GBs. Note that θ_1 and θ_2 are equal (θ_1 and θ_2 are defined in the right model of part a), leading to symmetric tilt GBs in polygonal GFs. (b) Four models showing the determination of GBs from one etched polygonal pattern without the knowledge of the GF morphology. The grains within GFs are marked by different colors, and the central white areas represent etched polygonal patterns. The outer polygons indicate the geometry of original polygonal GFs before etching. (c and d) Schematic diagrams showing the growth processes of polygonal GFs. Different grains are marked by different colors, and the corresponding interfaces define the path of GBs. (e−g) Typical SEM images of polygonal GFs showing the presence of white dots. Dashed lines are indicated in (e), and the crossing point is close to one white dot possibly acting as a nucleation site. (h) SEM image of hexagonal GFs grown on a precleaned Cu surface.

the formation of polygonal GFs are schematically illustrated in Figure 4c,d.

The model itself predicts several remarkable properties of GBs for polygonal GFs. The GBs are continuous and straight lines at a macroscopic scale. The physical starting point of the formation of a GB is geometrically located at the intersection point of GB lines depending on a specific model (Figure 4a). Most importantly, all the lines of GBs exactly bisect the corresponding angles of non-120° in polygonal GFs (see the strict proof in Figure S13), and therefore all GBs in our grown polygonal GFs are predicted to be symmetric tilt boundaries (see the right model of Figure 4a where equal θ_1 and θ_2 are indicated). Moreover, the misorientation angles between adjacent grains can also be derived from these models. Independently, the paths of more than 88 GBs in polygonal GFs were experimentally determined, and the two angles intersected by a GB are almost the same, with a deviation from the average value being less than 2.5%. In addition, several mis-orientation angles measured by experiments (Figure 3 and Figures S6−S8) perfectly matched those determined by the models. These results show excellent consistency with the prediction of the model, representing a key finding of this work.

Our approach using combined experimental and modeling studies unambiguously reveals the fundamental principle of how GBs are dynamically formed in CVD-grown polygonal GFs. Using this rule, the GB profile and misorientation angles between adjacent grains can be directly determined from geometries of polygonal GFs, thus providing a simple method for identification of both these critical parameters without the need for relying on any special techniques. With this simple method, we found that more than 90% of these misorientation angles are located between 10° and 30° (Figure S14). This empirical result is consistent with that from the previous reports,[13,15] indicating that there may exist a favored orientation for GFs grown on a Cu surface.

This model can be applied back to the case of graphene etching. Figure 4b shows several models where only one etched polygonal hole is present at the center of the GFs in the cases of bicrystal and tricrystal GFs. It can be clearly seen and concluded that the lines of GBs cross the vertex of non-120° angles in an etched polygon in two manners. When the angle is less than 120° (the upper two in Figure 4b), the GB exactly bisects it. When the angle is larger than 120°, the GB bisects the angle (the lower left of Figure 4b)

that subtracts a 60° angle. This shows that GBs can also be predicted by using one etched polygon in the case of a bicrystal. Even a tricrystal's GBs can be simply predicted (the lower right of Figure 4b). Figure S9h shows the central etched polygon and GF with a round etched perimeter. In this case, the prediction of GBs by using a central etched polygon is consistent with the experimentally determined lines. Note that this model is based on a regularly hexagonal GF growth. In practice, the underlying Cu substrate may introduce an anisotropic graphene growth rate along a different crystal direction.[31] In our grown GFs, this effect is small, leading to a perfect matching between model prediction and experimental results. Even in the presence of the anisotropic growth rate induced by a substrate, the prediction can in principle still be made by incorporating this effect in the model.

The developed approach for studying GB formation in a polygonal GF can be logically extended to the case of merging different GFs. Figure S15 shows the comparison between the results predicted by geometric models and obtained by experimental observations for three typical cases. In contrast to a simple straight line of a GB in a polygonal GF, the GB profile is characterized by a continuous polygonal line depending on the specific merging situation. Despite this, GB profiles determined by both methods are essentially consistent, demonstrating the universality of our approach.

Moreover, this model can provide insight into the graphene nucleation mechanism. For example, we repeatedly observed the existence of white dots close to the starting point of GBs on polygonal GFs. Figure 4e shows a white dot away from the central nucleus of a "mother" GF, and Figure 4f shows the aggregation of white dots that are close to the intersection point of multiple GBs. The results shown in Figure 4g demonstrate that a large aggregation of white dots tends to produce a more complex polygon containing many grains and GBs in GFs. These white dots were further confirmed to be mainly composed of silicon oxide, as shown in Figure S16. The existence of white dots is a general phenomenon in the system of graphene growth on Cu.[5,20−22] Regardless of the formation of SiO_2 in the CVD system, graphene nucleation preferentially occurs around these impurity sites. Remarkably, the location of the white dot beside the center one shown in Figure 4e is consistent with the starting point of GB formation predicted from the model, further confirming the validity of the model. This in principle provides a means to modulate the relative population of polygonal GFs. As an example, we electropolished a Cu surface to eliminate surface impurities before growth, and we found that most of the grown GFs were uniformly hexagon-shaped with a large size due to the reduction of the nucleation density originating from surface impurities (Figure 4h). Note that it is not necessary for nucleation sites to occur on visible white dots. It is also important to recognize that while the number of GB lines is directly associated with nucleation seed density of graphene in a polygonal GF, the formation of each GB line is essentially independent.

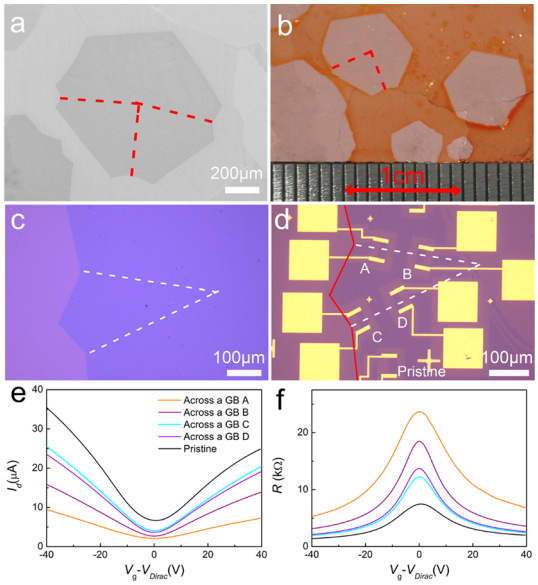

Figure 5. Growth control of GB length and the fabrication and characterization of FET devices. (a and b) SEM and photographic images of grown polygonal GFs with different GB lengths of 0.6 and 3 mm, respectively. (c) Optical image of a part polygonal GF for FET device fabrication, in which predicted GB lines are indicated by white dashed lines. (d) Optical image of fabricated graphene devices across GBs. Original GF shape and GBs are marked by red lines and white dashed lines, respectively. (e) Normalized transfer curves of five graphene FET devices shown in (d). The curves that correspond to pristine GBs and those across GBs are labeled in (e). (f) Corresponding resistance *versus* gate voltage curves of (e).

The understanding of graphene GB formation opens the door for controlling GB parameters in growth. As mentioned above, the numbers of GBs in a polygonal GF or relative population of GFs consisting of multiple grains *versus* those with single grain could be controlled by substrate treatment. In addition, it is possible to control misorientation angles of inner- or outer-merged grains by using Cu substrates with different surface facets. Importantly, the length of a straight GB line in polygonal GFs can be easily controlled by reducing graphene nucleation density and increasing growth time (Figure 5a,b, GB length up to 3 mm), thus allowing the straightforward and parallel fabrication of multiple GB-based electronic devices, which is otherwise difficult to realize by using randomly distributed, short and curved GBs normally found in previous studies. For example, previous activities involved the use of Raman mapping or dark-field TEM techniques to first locate GBs within graphene and then fabricate devices.[5,6] In contrast to these difficulties, many back-gated graphene FETs were directly fabricated on polygonal GFs within a single grain and across

geometrically predicted GBs on 300 nm SiO_2/Si substrates using electron beam lithography. Figure 5c shows an optical image of a transferred polygonal GF with predicted dashed lines of GBs prior to FET device fabrication. Figure 5d shows an optical image of four FET devices fabricated across the predicted GB lines. These devices have a channel length and width of 40 and 20 μm, respectively.

Figure 5e shows the transfer curves of devices measured within a single grain and across a GB. All devices show typical p-type graphene FET behaviors. In cases of devices measured on a single grain, device-to-device variation can be found. However, the conductance across a GB for all devices is less than that of a single grain at different carrier densities modulated by the back-gate voltage. The results for devices fabricated on another GF show a similar qualitative trend (Figure S17). The extracted hole mobility (2937−2973 $cm^2 V^{-1} s^{-1}$) within a grain is higher than those (800−2200 $cm^2 V^{-1} s^{-1}$) across a GB. Moreover, Figure 5f shows a plot of resistance as a function of gate voltage for devices. Note that all devices have the same geometric parameters. In addition, in order to reduce the effect of contact resistance for comparison of different devices, graphene devices with Hall-bar structure were fabricated (Figure S18a and b). The result of electrical tests on these devices shows that sheet resistances crossing a GB are higher than those without passing a GB (Figure S18c and d). These results clearly show that the GB provides an extra resistance, which is qualitatively consistent with previous results measured on those across an intergrain GB.[5,6,32]

CONCLUSION

In summary, we have discovered a general geometric rule describing how GBs are dynamically formed in polygonal GFs grown by a typical CVD method. Using this rule, the key parameters of GBs such as profile and the misorientation angles between adjacent graphene grains can be directly determined by geometries of polygonal GFs. Besides the demonstrated parallel fabrication of FET devices across GBs, long straight GB lines should also find wide use in the fundamental study of graphene GB properties and various GB-based electronic devices. This work presents a significant step toward engineering grains and GBs in graphene growth.

METHODS

Graphene Growth and Etching. We synthesized graphene by CVD on both solid Cu foils and liquid Cu/W foils. First, Cu foil was put into a 1 in. quartz tube and heated to 1070−1100 °C in a 8−20 sccm H_2 and 240 sccm Ar mixed atmosphere within 30 min. Next, 0.5−3 sccm diluted CH_4 (0.5% balanced in Ar) was introduced into the CVD system for several to dozens of hours for graphene growth. Finally, the CVD system was slowly cooled to 700 °C and then quickly cooled to room temperature. In the case of graphene etching, as-grown graphene was exposed in a fixed H_2/Ar atmosphere for 1 to 10 min immediately after turning off CH_4 flow while keeping the temperature unchanged.

Graphene FET Device Fabrication. The as-grown GFs on solid Cu and liquid Cu were transferred onto 300 nm SiO_2/Si substrates by wet-etching or electrochemical delamination methods. The selected areas of transferred graphene on SiO_2/Si substrates were first cut into 40-μm-long, 20-μm-wide microribbons by e-beam lithography and oxygen plasma etching. Then the contact electrodes (Ti/Au: 5 nm/50 nm) were patterned by e-beam lithography and source/drain electrodes were deposited using thermal evaporation. The mobility of charge carriers is extracted from the equation

$$\mu_{dev} = \frac{L}{V_D C_{ox} W} \frac{dI_d}{dV_g}$$

where L and W are the device channel length and width, V_D is the voltage between source and drain electrodes, and C_{ox} is the gate capacitance per unit area.

Characterizations. The morphology and structure of graphene were characterized with optical microscopy, Raman spectroscopy (Renishaw inVia Plus, with laser excitation at 514 nm and a spot size of 1−2 μm), field emission SEM (Hitachi S-4800 at 1 kV), TEM (JEM-2011 at 120 kV), and high-resolution TEM (JEM-ARM200F at 80 kV). Electrical measurements were performed at room temperature in air using a semiconductor characterization system (Keithley 4200-SCS).

Conflict of Interest: The authors declare no competing financial interest.

Supporting Information Available: Additional figures. The Supporting Information is available free of charge on the ACS Publications website at DOI: 10.1021/acsnano.5b01827.

Acknowledgment. This work was supported by the National Basic Research Program of China (2011CB932700, 2013CB933504, 2013CBA01602, and 2011CB932303), the National Natural Science Foundation of China (61171054, 21273243, 60911130231, 51233006, and 61390502), and the Strategic Priority Research Program of the Chinese Academy of Sciences (XDB12030100). The authors thank Ms. Jie Xu for help with TEM measurements.

REFERENCES AND NOTES

1. Novoselov, K. S.; Geim, A. K.; Morozov, S. V.; Jiang, D.; Zhang, Y.; Dubonos, S. V.; Grigorieva, I. V.; Firsov, A. A. Electric Field Effect in Atomically Thin Carbon Films. *Science* **2004**, *306*, 666–669.
2. Yazyev, O. V.; Louie, S. G. Electronic Transport in Polycrystalline Graphene. *Nat. Mater.* **2010**, *9*, 806–809.
3. Ihnatsenka, S.; Zozoulenko, I. V. Electron Interaction, Charging, and Screening at Grain Boundaries in Graphene. *Phys. Rev. B* **2013**, *8*, 085436.
4. Geim, A. K. Graphene: Status and Prospects. *Science* **2009**, *324*, 1530–1534.
5. Yu, Q. K.; Jauregui, L. A.; Wu, W.; Colby, R.; Tian, J.; Su, Z.; Cao, H.; Liu, Z.; Pandey, D.; Wei, D.; *et al*. Control and Characterization of Individual Grains and Grain Boundaries in Graphene Grown by Chemical Vapour Deposition. *Nat. Mater.* **2011**, *10*, 443–449.
6. Tsen, A. W.; Brown, L.; Levendorf, M. P.; Ghahari, F.; Huang, P. Y.; Havener, R. W.; Ruiz-Vargas, C. S.; Muller, D. A.; Kim, P.; Park, J. Tailoring Electrical Transport across Grain Boundaries in Polycrystalline Graphene. *Science* **2012**, *336*, 1143–1146.
7. Grantab, R.; Shenoy, V. B.; Ruoff, R. S. Anomalous Strength Characteristics of Tilt Grain Boundaries in Graphene. *Science* **2010**, *330*, 946–948.

8. Lee, G. H.; Cooper, R. C.; An, S. J.; Lee, S.; van der Zande, A.; Petrone, N.; Hammerberg, A. G.; Lee, C.; Crawford, B.; Oliver, W.; *et al*. High-Strength Chemical-Vapor-Deposited Graphene and Grain Boundaries. *Science* **2013**, *340*, 1073–1076.
9. Wei, Y.; Wu, J.; Yin, H.; Shi, X.; Yang, R.; Dresselhaus, M. The Nature of Strength Enhancement and Weakening by Pentagon-Heptagon Defects in Graphene. *Nat. Mater.* **2012**, *11*, 759–763.
10. Ovid'ko, I. A. Review on Grain Boundaries in Graphene. Curved Poly- and Nanocrystalline Graphene Structures as New Carbon Allotropes. *Rev. Adv. Mater. Sci.* **2012**, *30*, 201–224.
11. Duong, D. L.; Han, G. H.; Lee, S. M.; Gunes, F.; Kim, E. S.; Kim, S. T.; Kim, H.; Ta, Q. H.; So, K. P.; Yoon, S. J.; *et al*. Probing Graphene Grain Boundaries with Optical Microscopy. *Nature* **2012**, *490*, 235–239.
12. Ly, T. H.; Duong, D. L.; Ta, Q. H.; Yao, F.; Vu, Q. A.; Jeong, H. Y.; Chae, S. H.; Lee, Y. H. Nondestructive Characterization of Graphene Defects. *Adv. Funct. Mater.* **2013**, *23*, 5183–5189.
13. Huang, P. Y.; Ruiz-Vargas, C. S.; van der Zande, A. M.; Whitney, W. S.; Levendorf, M. P.; Kevek, J. W.; Garg, S.; Alden, J. S.; Hustedt, C. J.; Zhu, Y.; *et al*. Grains and Grain Boundaries in Single-Layer Graphene Atomic Patchwork Quilts. *Nature* **2011**, *469*, 389–392.
14. Kim, K.; Lee, Z.; Regan, W.; Kisielowski, C.; Crommie, M. F.; Zettl, A. Grain Boundary Mapping in Polycrystalline Graphene. *ACS Nano* **2011**, *5*, 2142–2146.
15. An, J.; Voelkl, E.; Suk, J. W.; Li, X.; Magnuson, C. W.; Fu, L.; Tiemeijer, P.; Bischoff, M.; Freitag, B.; Popova, E.; *et al*. Domain (Grain) Boundaries and Evidence of "Twinlike" Structures in Chemically Vapor Deposited Grown Graphene. *ACS Nano* **2011**, *5*, 2433–2439.
16. Yasaei, P.; Kumar, B.; Hantehzadeh, R.; Kayyalha, M.; Baskin, A.; Repnin, N.; Wang, C.; Klie, R. F.; Chen, Y. P.; Kral, P.; *et al*. Chemical Sensing with Switchable Transport Channels in Graphene Grain Boundaries. *Nat. Commun.* **2014**, *5*, 4911–4918.
17. Kim, K.; Lee, H. B.; Johnson, R. W.; Tanskanen, J. T.; Liu, N.; Kim, M. G.; Pang, C.; Ahn, C.; Bent, S. F.; Bao, Z. Selective Metal Deposition at Graphene Line Defects by Atomic Layer Deposition. *Nat. Commun.* **2014**, *5*, 4781–4789.
18. Van der Zande, A. M.; Huang, P. Y.; Chenet, D. A.; Berkelbach, T. C.; You, Y.; Lee, G. H.; Heinz, T. F.; Reichman, D. R.; Muller, D. A.; Hone, J. C. Grains and Grain Boundaries in Highly Crystalline Monolayer Molybdenum Disulphide. *Nat. Mater.* **2013**, *12*, 554–561.
19. Najmaei, S.; Liu, Z.; Zhou, W.; Zou, X.; Shi, G.; Lei, S.; Yakobson, B. I.; Idrobo, J. C.; Ajayan, P. M.; Lou, J. Vapour Phase Growth and Grain Boundary Structure of Molybdenum Disulphide Atomic Layers. *Nat. Mater.* **2013**, *12*, 754–759.
20. Wu, B.; Geng, D.; Guo, Y.; Huang, L.; Xue, Y.; Zheng, J.; Chen, J.; Yu, G.; Liu, Y.; Jiang, L.; *et al*. Equiangular Hexagon-Shape-Controlled Synthesis of Graphene on Copper Surface. *Adv. Mater.* **2011**, *23*, 3522–3525.
21. Geng, D.; Wu, B.; Guo, Y.; Huang, L.; Xue, Y.; Chen, J.; Yu, G.; Jiang, L.; Hu, W.; Liu, Y. Uniform Hexagonal Graphene Flakes and Films Grown on Liquid Copper Surface. *Proc. Natl. Acad. Sci. U.S.A.* **2012**, *109*, 7992–7996.
22. Wu, B.; Geng, D.; Xu, Z.; Guo, Y.; Huang, L.; Xue, Y.; Chen, J.; Yu, G.; Liu, Y. Self-Organized Graphene Crystal Patterns. *NPG Asia Mater.* **2013**, *5*, e36.
23. Geng, D.; Wu, B.; Guo, Y.; Luo, B.; Xue, Y.; Chen, J.; Yu, G.; Liu, Y. Fractal Etching of Graphene. *J. Am. Chem. Soc.* **2013**, *135*, 6431–6434.
24. Zhang, Y.; Li, Z.; Kim, P.; Zhang, L.; Zhou, C. Anisotropic Hydrogen Etching of Chemical Vapor Deposited Graphene. *ACS Nano* **2012**, *6*, 126–132.
25. Ma, T.; Ren, W.; Zhang, X.; Liu, Z.; Gao, Y.; Yin, L. C.; Ma, X. L.; Ding, F.; Cheng, H. M. Edge-Controlled Growth and Kinetics of Single-Crystal Graphene Domains by Chemical Vapor Deposition. *Proc. Natl. Acad. Sci. U.S.A.* **2013**, *110*, 20386–20391.
26. Liu, Y.; Yakobson, B. I. Cones, Pringles, and Grain Boundary Landscapes in Graphene Topology. *Nano Lett.* **2010**, *10*, 2178–2183.
27. Yazyev, O. V.; Louie, S. G. Topological Defects in Graphene: Dislocations and Grain Boundaries. *Phys. Rev. B* **2010**, *81*, 195420.
28. Nguyen, V. L.; Shin, B. G.; Duong, D. L.; Kim, S. T.; Perello, D.; Lim, Y. J.; Yuan, Q. H.; Ding, F.; Jeong, H. Y.; Shin, H. S.; *et al*. Seamless Stitching of Graphene Domains on Polished Copper (111) Foil. *Adv. Mater.* **2014**, *27*, 1376–1382.
29. Shu, H.; Chen, X.; Tao, X.; Ding, F. Edge Structural Stability and Kinetics of Graphene Chemical Vapor Deposition Growth. *ACS Nano* **2012**, *6*, 3243–3250.
30. Gao, J.; Zhao, J.; Ding, F. Transition Metal Surface Passivation Induced Graphene Edge Reconstruction. *J. Am. Chem. Soc.* **2012**, *134*, 6204–6209.
31. Meca, E.; Lowengrub, J.; Kim, H.; Mattevi, C.; Shenoy, V. B. Epitaxial Graphene Growth and Shape Dynamics on Copper: Phase-Field Modeling and Experiments. *Nano Lett.* **2013**, *13*, 5692–5697.
32. Jauregui, L. A.; Cao, H.; Wu, W.; Yu, Q.; Chen, Y. P. Electronic Properties of Grains and Grain Boundaries in Graphene Grown by Chemical Vapor Deposition. *Solid State Commun.* **2011**, *151*, 1100–1104.